Mesenchymal stem cell-mediated delivery of the sodium iodide symporter supports radionuclide imaging and treatment of breast cancer

Running Title: MSC mediated imaging and therapy of Breast Cancer

Title: Mesenchymal Stem Cell (MSC) mediated delivery of the Sodium Iodide Symporter (NIS) supports radionuclide imaging and treatment of breast cancer

Authors: Roisin M. Dwyer[1,4], James Ryan[1], Ronan J. Havelin[5], John C. Morris[6], Brian W. Miller[7], Zhonglin Liu[7], Richard Flavin[3], Cathal O'Flatharta[4], Mark J. Foley[5], Harrison H. Barrett[7], J. Mary Murphy[4], Frank P. Barry[4], Timothy O'Brien[2,4] and Michael J. Kerin[1].

Institutions: Disciplines of Surgery[1], Medicine[2], and Pathology[3], School of Medicine, Regenerative Medicine Institute[4] and School of Physics[5], National University of Ireland Galway, Ireland. Division of Endocrinology[6], Mayo Clinic, Rochester, Minnesota, USA. Department of Radiology and Center for Gamma-Ray Imaging[7], University of Arizona, Tucson, Arizona, USA.

Author Contribution Summary:

Roisin Dwyer: Conception and design, Financial support, Collection and/or assembly of data, Data analysis and interpretation, Manuscript writing, Final approval of manuscript

James Ryan: Collection and/or assembly of data, Data analysis and interpretation

Ronan Havelin: Collection and/or assembly of data, Data analysis and interpretation, Final approval of manuscript

John Morris: Provision of study material, Data analysis and interpretation, Final approval of manuscript

Brian Miller: Data analysis and interpretation

Zhonglin Liu: Data analysis and interpretation, Final approval of manuscript

Richard Flavin: Data analysis and interpretation

Cathal O'Flatharta: Conception and design

Mark Foley: Conception and design, Final approval of manuscript

Harrison Barrett: Conception and design, Data analysis and interpretation, Final approval of manuscript

J. Mary Murphy: Conception and design, Provision of study material, Data analysis and interpretation

Frank Barry: Conception and design, Provision of study material, Data analysis and interpretation

Timothy O'Brien: Conception and design, Provision of study material, Data analysis and interpretation, Final approval of manuscript

Michael Kerin: Conception and design, Financial support, Data analysis and interpretation, Final approval of manuscript

Corresponding Author: Roisin M Dwyer, PhD, Division of Surgery, School of Medicine, National University of Ireland Galway, Galway, Ireland. **Phone:** +353 91 544637

Fax: +353 91 494509 **E-mail:** roisin.dwyer@nuigalway.ie

Funding Acknowledgement: RMD-Health Research Board of Ireland (RP2007/197); JR- Cancer Research Ireland (CRI07/DWY); COF, TOB, FPB, JMM- Science

Foundation Ireland, General- National Breast Cancer Research Institute. Center for Gamma-Ray Imaging - National Institute for Biomedical Imaging and Bioengineering (P41-EB002035)

Keywords/phrases: Sodium Iodide Symporter (NIS); Mesenchymal Stem Cell (MSC); Breast Cancer; Gene therapy; In vivo Imaging; Radiotherapy

Abstract

Mesenchymal Stem Cells (MSCs) migrate specifically to tumors in vivo, and coupled with their capacity to bypass immune surveillance, are attractive vehicles for tumor-targeted delivery of therapeutic agents. This study aimed to introduce MSC-mediated expression of the sodium iodide symporter (NIS) for imaging and therapy of breast cancer. Tumor bearing animals received an intravenous or intratumoral injection of NIS expressing MSCs (MSC-NIS), followed by $^{99m}TcO_4^-$ imaging 3-14Days (D) later using a BazookaSPECT γ-camera. Tissue was harvested for analysis of hNIS expression by RQ-PCR. Therapy animals received an intraperitoneal injection of ^{131}I or saline 14D following injection of MSC-NIS, and tumor volume was monitored for 8 weeks. BazookaSPECT imaging following injection of MSC-NIS revealed an image of animal intestines and chest area at D3, with a weak tumor image also visible. By D14, the tumor was visible with a significant reduction in radionuclide accumulation in non-target tissue observed. hNIS gene expression was detected in the intestines, heart, lungs and tumor at early timepoints but later depleted in non-target tissues and persisted at the tumor site. Based on imaging/biodistribution data, animals received a therapeutic dose of ^{131}I 14D following MSC-NIS injection. This resulted in a significant reduction in tumor growth (Mean ± SEM, 236 ± 62mm^3 versus 665 ± 204 mm^3 in controls). The ability to non-invasively track MSC migration and transgene expression in real time prior to therapy is a major advantage to this strategy. This promising data supports the feasibility of this approach as a novel therapy for breast cancer.

Introduction

Mesenchymal Stem Cells (MSCs) are non-haematopoietic multipotent cells that can be isolated and expanded with relative ease from a number of different sources, including bone marrow and adipose tissue [1, 2]. They are defined by a panel of specific cell surface antigens [3], and an innate ability to differentiate along multiple lineages including osteogenic, chondrogenic and adipogenic [4]. Although MSCs play a primary role in tissue regeneration [5, 6], they also have the proven ability to migrate specifically to the site of multiple tumor types in vivo [7, 8]. When combined with their capacity to bypass host immune surveillance [9, 10], this makes MSCs attractive vehicles for tumor-targeted delivery of therapeutic agents and their biological products, with promising results reported in a range of tumor types [8, 11].

This is particularly promising for metastatic disease, as the majority of cancer-related deaths occur as a result of complications of metastasis. In the case of breast cancer, the mortality rate in women overall is second only to lung cancer, with >39,000 deaths anticipated in the US in 2010 [12]. In this context, previous studies have demonstrated targeted MSC-mediated delivery of conditionally replicating adenovirus [13] or interferon-β [14] to lung metastases of breast cancer in vivo, showing a significant therapeutic effect. We have also previously reported MSC engraftment in nodal metastases of breast cancer in vivo [15]. One of the major challenges to this approach is lack of understanding of MSC-tumor tropism, and the potential for non-specific targeting of healthy tissue. The ability to dynamically image MSC migration and engraftment in real time, to confirm tumor targeting is essential to increase understanding of this process and provide for translation to the clinical setting.

The ability of the thyroid gland to concentrate iodide is based on expression of the Sodium Iodide Symporter (NIS), and forms the basis for radiolabeled iodide imaging and treatment of thyroid disease. A major advantage to the approach is the ability to non-invasively image uptake of a tracer such as ^{99m} Technetium pertechnetate ($^{99m}TcO_4^-$) or ^{123}Iodide (^{123}I) prior to administration of a therapeutic dose of ^{131}I. Due to the safety and efficacy of this approach in imaging and treatment of thyroid disease [16], there have been a number of studies reporting successful introduction of ectopic NIS expression to support imaging and therapy of non-thyroidal malignancies [17, 18]. However, the major limitation of current NIS delivery and gene therapy in general, is lack of tumor targeting. A potential way to overcome this is through the use of MSCs as cellular vehicles. NIS-transduced MSCs could potentially provide for noninvasive imaging to track MSC homing and engraftment at the tumor site. Due to the pathlength of ^{131}I, successful engraftment of NIS-expressing MSCs may potentially also provide for ablation of surrounding tumor cells mediated by the bystander effect of the radionuclide [19].

To date, the majority of MSC biodistribution studies have relied on invasive techniques such as tissue biopsy followed by immunohistochemistry or PCR. In the case of NIS, as opposed to direct cell labelling, functional uptake of tracer is dependent on cell viability, and NIS itself is a non-toxic, non-immunogenic protein. There have been a number of studies tracking MSC migration to tumors in vivo, employing expression of a reporter gene in conjunction with bioluminescent or PET imaging [20-24]. Recently, NIS has been used as a reporter gene in neural [25-27], cardiac [28], hematopoietic[29] and mesenchymal stem cells [25]. While these studies support the feasibility of this approach, the significant

advantage of NIS having the potential to serve as both a reporter and therapeutic gene has yet to be exploited.

The aim of this study was to introduce functional NIS expression into MSCs and determine whether systemic administration to tumor bearing animals would result in sufficient engraftment to permit radionuclide imaging. Following functional imaging, the feasibility of radioiodide therapy of tumors based on the bystander effect from NIS-expressing MSCs was also investigated.

Materials and Methods

Isolation and Culture of Mesenchymal Stem Cells (MSCs)

MSCs were isolated from bone marrow aspirates of healthy volunteers with informed consent by direct plating using a defined clinical protocol. Cells were cultured for 12-15 days to deplete the non-adherent haematopoietic cell fraction and maintained in alpha Modified Eagle's Medium (α-MEM) supplemented with pre-selected FBS (10%) and 100 IU/ml Penicillin/100µg/ml Streptomycin. The ability of MSCs to differentiate into chondrocytes, adipocytes and osteoblasts was confirmed prior to use. Characterization of surface receptors was performed targeting the markers CD105, CD73, CD90 (positive) and CD34, CD45 (negative).

Adenoviral Infection of MSCs

A replication-deficient human recombinant adenovirus serotype 5 construct containing human NIS under the control of the cytomegalovirus (CMV) promoter (AdNIS) was used [30]. MSCs suspended in serum-free medium were centrifuged in the presence of virus for

90 mins at 2000 x *g*. Following infection the pellet of cells was rinsed in serum free medium and resuspended in complete medium for culture as required. Transduction efficiency was determined using the GFP reporter gene. GFP expression was visualised 48hrs following infection with Ad5/CMV/GFP (Vector Biolabs) using fluorescence microscopy (Olympus BX60), and quantified by flow cytometry using a Guava® EasyCyte™ 8HT flow cytometer.

Detection of NIS Expression

At a variety of timepoints (3-28 days) following infection with Adenovirus (multiplicity of infection (MOI) 0-200), total RNA was extracted from cells using the RNeasy® Mini Kit (QIAGEN Ltd.) following manufacturer's protocol. RNA (1µg) was reverse transcribed using SuperScript III reverse transcription enzyme (Invitrogen). cDNA samples were amplified and analyzed by relative quantitative-PCR (RQ-PCR) using the ABI Prism 7000 sequence detector system (Applied Biosystems). PreDeveloped Taqman® Assay Reagents (PDARS) specific to *hNIS (Solute Carrier 5, member 5; SLC5A5)* and the endogenous control, *Peptidyl-Prolyl Isomerase A (PPIA)* were used. The comparative C_T method was used to quantify expression of *hNIS* normalized to *PPIA*, with the levels expressed relative to untransfected cells. Changes in NIS expression were expressed using the $2^{-\Delta\Delta CT}$ method [31] and the fold change in triplicate experiments was recorded and presented as Mean ± SEM.

To detect protein expression, adenovirus infected or control cells were plated into 2-chamber slides. Three days later slides were put on ice for 15 mins and cells fixed in ice cold methanol at –20°C for 15 mins. NIS protein expression and localization was

detected by immunohistochemistry using a monoclonal antibody [32] and a Discovery™ RedMAP Kit on a Discovery™ Ventana system. Slides were then washed in warm soapy water to remove oil, followed by rinsing in ddH_20 and sequential treatment as follows: 3 mins in 75% alcohol, 3 mins in 95% alcohol, 3 mins in 100% alcohol, and 2 serial immersions of 3mins in Xylene. The slides were then mounted in DPX mounting medium and analyzed using an Olympus BX60 microscope and analySIS Soft Imaging System.

^{125}I Uptake studies

The ability of MSCs to concentrate iodide at various timepoints (1-7 days) following adenovirus infection was determined as previously described [33]. Briefly, after transfection, cells were incubated in HBSS containing 10 mmol/L HEPES, 10 μmol/L NaI and 0.1 μCi $Na^{125}I$/mL (pH 7.3), and 10 μmol/L $KClO_4$, a competitive inhibitor of iodide uptake by NIS, was included in control wells. After a 45-min incubation at 37°C, cells were washed with ice-cold PBS, lysed with 1 mol/L NaOH, and concentrated iodide measured on a γ-counter.

Tumor growth and MSC administration

Female athymic nude mice (Harlan Sprague-Dawley, Indianapolis, IN) received a subcutaneous right flank injection of 2 x 10^7 MDA-MB-231 cells in 0.2 mL 50% Matrigel/Leibowitz-15 medium. When tumors had reached an appropriate volume (~100 mm^3), mice received either an intratumoral (n=24 in total) or intravenous injection of 1 x 10^6 AdNIS infected MSCs suspended in 50 μl DMEM (Figure 1). For intratumoral injection, the needle tip was inserted and then retracted as the cells were injected,

followed by repositioning in another area of the tumor to increase cell dispersal. These groups were subdivided into a therapy study and a biodistribution study. A further two groups of animals (n=6 each) received either no MSC injection, or an intravenous injection of naked AdNIS (no MSCs). Seven days prior to administration of radionuclide ($^{99m}TcO_4^-$ or ^{131}I), animals were placed on a low-iodine diet with Thyroxine (T_4)-supplemented water (5 mg/L) to reduce thyroidal uptake of radionuclides (Figure 1). All animal experiments were licensed, and carried out according to the guidelines of the Institutional Animal Ethics Committee. Experiments involving radionuclides were approved by the Radiological Protection Institute of Ireland, and performed according to institutional guidelines.

In vivo biodistribution of NIS-expressing MSCs

- **$^{99m}TcO_4^-$ imaging of NIS-transfected MSCs *in vivo***

3-14 days following administration of MSC-NIS, tumor bearing animals were given an intraperitoneal injection of 2 mCi/74 MBq technetium-99m pertechnetate ($^{99m}TcO_4^-$, Figure 1). One hour later animals were anaesthetized with a ketamine/xylazine cocktail and images acquired using a BazookaSPECT γ-camera [34].The BazookaSPECT system consists of a 1 mm pinhole collimator, a 600 μm Hamamatsu caesium iodide (CsI) scintillator, an image intensifier, an optical system and a charge-coupled device (CCD) camera. A rotating platform supported capture of SPECT data, with a total of 30 images acquired in 12º steps over a full rotation. Planar imaging was also performed with an acquisition time of 15 mins. Data were acquired using a LabView interface (National Instruments) and stored using a list-mode method. The volume data were reconstructed

using 0.5 – 2.0 mm voxels. The dose of tracer accumulated at each site was estimated and expressed as a percentage of the total administered dose. Regions of interest (ROIs) were drawn around all visible organs and the whole body. After correction for background activity, the level of uptake in each area was expressed as a percentage of the total activity in the mouse.

- **Gene Expression**

3 and 7 days following administration of MSC-NIS or naked virus (AdNIS) to tumor bearing animals, mice were sacrificed by CO_2 inhalation and organs harvested for analysis by RQ-PCR. The following organs were retrieved: heart, lungs, liver, spleen, kidneys, stomach, large/small intestine, and tumor. Tissues were immediately immersed in RNAlater® (Ambion, Inc), and then stored at -80°C until required. Prior to RNA extraction, tissue was homogenized briefly in 1ml TRIzol® Reagent (Invitrogen) using a Polytron PT 1600 E @ 30,000 rpm. RNA was extracted and analysed by RQ-PCR as described for cultured cells. Targets included *NIS* (human and mouse specific PDARs), human *MRPL19* (endogenous control for human cells) and mouse *β-actin* (endogenous control for mouse cells).

***In vivo* ^{131}I Therapy**

Fourteen days following intravenous (n=12) or intratumoral (n=12) administration of MSC-NIS to tumor bearing animals, mice were given an intraperitoneal injection of 1 mCi/37 MBq ^{131}I (n=6 of each group) or saline (n=6 of each group, Figure 1). Tumor

volume was monitored twice weekly for 8 weeks using calipers, and estimated according to the formula: volume (mm^3) = L x W x D x 0.52.

Histology and Immunohistochemistry

Eight weeks following administration of ^{131}I or saline, animals were sacrificed by CO_2 inhalation and tumors harvested. Tissue was immersed in 4% paraformaldehyde for 24 hrs, transferred to 30% sucrose for 24 hrs, snap frozen in an isopentane/liquid nitrogen bath and stored at -80ºC until required for cryosectioning. Frozen tissue samples from xenografts were cryosectioned (5 µm sections) and allowed to air dry at RT followed by rehydration in PBS-0.05% Tween-20. Sections were then stained with Haematoxilyn and Eosin (H & E) or prepared for immunohistochemistry as described. Following blocking of endogenous peroxidases, antigen retrieval was performed using citrate buffer. Sections were probed with a polyclonal antibody to Proliferating Cell Nuclear Antigen (PCNA, AbCAM). A HRP-conjugated secondary antibody was employed followed by detection using a peroxidase substrate kit containing the chromogen diaminobenzidine (Vector Laboratories). Cells were counterstained with Haematoxylin. Once staining was complete sections were washed in warm soapy water, dehydrated in serial alcohol immersions, and mounted using DPX mounting medium.

Results

***In vitro* NIS expression and function following adenovirus infection of MSCs**

Adenovirus containing GFP was used to determine transduction efficiency and optimize viral infection conditions. Visualization of cells from two individual donors using a

fluorescent microscope revealed that the majority of the cell populations were strongly positive for GFP following transfection (Figure 2A(i)-(ii)). Quantification of GFP positive cells by flow cytometry demonstrated a transduction efficiency of 85-92% at an MOI of 100, with no significant benefit gained from increasing the MOI to 200.

NIS gene expression in MSCs 72 hrs following adenovirus infection was confirmed at a MOI of 50-200 using RQ-PCR (Figure 2B). Robust gene expression was detected with a mean 3.9 Log fold increase over uninfected cells at MOI 100.

The ability of transduced MSCs to concentrate iodide (^{125}I) was determined at a variety of timepoints (1-7 days) following infection at a range of MOIs (Figure 2C). Iodide uptake studies revealed efficient NIS function, with a 27-60 fold increase in uptake at MOIs ranging from 50-200. Inclusion of the NIS inhibitor perchlorate ($KCLO_4$) in wells resulted in 70-85% inhibition of iodide uptake, confirming specificity (Figure 2C). NIS expression and function remained significantly elevated 7 days following infection. Further analysis of NIS gene expression at later timepoints following adenoviral infection, revealed persistence of robust expression up to 28 days later (Figure 2D). There was no significant difference in NIS expression or function detected between cells infected at MOI 100 or 200, and so subsequent infections were performed at MOI 100.

In vivo Imaging of MSC-NIS engraftment

3-14 days following intravenous injection of MSC-NIS, animals received an intraperitoneal injection of $^{99m}TcO_4^-$ and imaging was performed using a BazookaSPECT γ-camera (Figure 3). In control animals that had received no injection of MSC-NIS, a pattern of uptake correlating with native NIS expression was observed, with $^{99m}TcO_4^-$ concentrated in the thyroid/salivary gland and stomach (Figure 3A). Three days following

intratumoral injection of MSC-NIS robust uptake of tracer at the tumor site was observed (Figure 3B). Following IV administration of MSC-NIS, an image of animal intestines was also observed at Day 3 (Figure 3C), with some diffuse uptake also seen in the chest area. A weak image of the right flank tumor was also visible (Figure 3C). By Day 14, uptake of tracer was visible at the site of the tumor with a significant reduction in accumulation in non-target tissue observed (Figure 3D). The bladder was also visible in some images as a result of tracer excretion in urine. Based on ROI readings, levels of tracer accumulation in areas of interest were expressed as a percentage of total administered dose. Levels of accumulation in the thyroid and stomach remained similar at Day 3 (1% thyroid, 14.7% stomach) and Day 14 (2.3% thyroid, 15.9% stomach). At Day 3, 18% of tracer was accumulated in intestines, and had reduced to non-significant levels by Day 14. Accumulation at the tumor site was estimated at 1.2% on Day 3 (Figure 3(C)), increasing to 9.4% by Day 14 (Figure 3(D)).

RQ-PCR detection of NIS expression in harvested tissues

Three and seven days following IV injection of MSC-NIS or adenovirus alone (AdNIS), animals were sacrificed and organs harvested for detection of *NIS* expression by RQ-PCR (Table 1). The species specific human endogenous control *MPRL19* was included as an indicator of the presence of human cells (engrafted MSCs) in tissues. As expected, *MRPL19* was detected in the tumors established using human cells, but was not detected in any other tissue when virus alone was administered. There was no detectable *hNIS* expression at the tumor site although it was detected in animal heart, lungs and liver at Day 3, but was no longer present at Day 7 (Table 1).

Three days following administration of MSC-NIS, *hNIS* was detected in tumor, heart, lungs, liver and large intestine tissue. Excluding liver, *MRPL19* was also detected in these tissues, indicating the presence of engrafted human MSCs. In the case of liver tissue, no *MRPL19* was detected suggesting that *NIS* expression was due to free virus and not MSC engraftment. In line with this, *NIS* was no longer detected in liver tissue at Day 7. While expression of *NIS/MRPL19* was depleted by Day 7 in heart, lungs and liver, the level was maintained at the tumor site (Table 1).

In vivo ^{131}I Therapy

Animals received an intraperitoneal injection of 1 mCi/37 MBq ^{131}I or saline 14 days following intratumoral (IT) or intravenous (IV) injection of MSC-NIS. In control animals (no MSC injection) and those that received MSC-NIS IV without ^{131}I therapy, tumor volume continued to increase rapidly throughout the 8 weeks of monitoring, with no significant difference in volume detected between the two groups (Figure 4). In animals that received IT injections of MSC-NIS followed by saline or ^{131}I, there was an apparent reduction in the rate of tumor growth from week 3 onwards (5 weeks following MSC injection), although no significant difference in tumor volume between treated (Mean ± SEM, 473 ± 80 mm^3) and untreated (391 ± 124 mm^3) animals was detected. The greatest impact of intervention was observed in animals that received an IV injection of MSC-NIS followed by ^{131}I 14 days later, which resulted in a significant reduction in tumor growth rate and final volume (236 ± 62 mm^3), compared to control animals (IV MSC-NIS + saline, 953 ± 189 mm^3).

Histology and Immunohistochemistry

Hematoxylin and Eosin (H & E) staining revealed extensive necrotic areas in tumors harvested from animals that received ^{131}I therapy 14 days following MSC-NIS delivery, but not control tumors (Figure 5A (i)-(iv)). This was observed irrespective of the route of MSC-NIS delivery, with an example of control and treated tumors following intravenous (Figure 5A (i)-(ii)) or intratumoral (Figure 5A (iii)-(iv)) delivery of MSC-NIS shown. Areas of necrosis in tissue from treated animals were quantified at 20-80% (Range) of total section area. Further analysis of tissue sections using a monoclonal antibody targeting the proliferative marker PCNA was also performed. In support of H & E findings, in tumors from control animals (no ^{131}I treatment) most cell nuclei were positive for PCNA, indicating the presence of actively proliferating cells (Figure 5B (i), (iii)). In contrast, tumors from treated animals stained weakly for PCNA (Figure 5B (ii), (iv).

Discussion

The current study describes the use of MSCs as cellular vehicles for breast tumor-targeted delivery of NIS, supporting dynamic radionuclide imaging and therapy of the disease.

Correct posttranslational targeting of NIS to the cell membrane is required for function, and concentrated iodide must be retained within the cell long enough to be therapeutically effective [35]. The results presented demonstrate membrane targeted and functional NIS expression following adenoviral infection of MSCs. It is noteworthy that NIS function was found to persist relatively long term in vitro, with robust iodide uptake still detected 7 days following infection. Since adenovirus mediated gene expression is

transient, peak expression is usually detected within 3-5 days following infection [36-38]. However in this case gene expression was found to persist for up to 28 days and further investigation revealed this was related to cell proliferation. MSCs undergo cell contact mediated inhibition of growth which resulted in persistent gene expression. When cells were passaged following infection, NIS expression and function decreased and were found to be inversely related to expression of the proliferative marker, Ki67 (results not shown).

In the current study investigation of MSC-NIS biodistribution following systemic infusion revealed engraftment in lungs, heart, intestine and tumor within a few days of administration. This concurs with previous reports showing initial ectopic engraftment in non-target tissues, particularly the lungs [20, 39]. However at later timepoints while detection of engraftment depleted elsewhere, the cells persisted at the tumor site. It is very encouraging that the level of IV infused MSC-NIS engraftment at the tumor site was high enough to support concentration of sufficient tracer to generate a signal over background. RQ-PCR analysis of tissues harvested following γ-camera imaging supported this data, with robust human NIS expression detected at the tumor site. While NIS expression depleted in non-target tissues by D7, gene expression persisted in tumor tissue. hNIS was not detected in the liver or spleen of these animals, with very low levels detected in the heart and lungs. When AdNIS was administered alone, ectopic hNIS expression was detected in multiple tissues including liver, lungs, spleen and kidney, highlighting efficient tumor targeting of MSCs. The data further highlights the importance of tracking MSC migration in real time, and the advantage of being able to perform a pretherapy scan to confirm tumor targeted MSC-NIS engraftment before administration of ^{131}I. The

persistent functional NIS expression at Day 14 also supported in vitro observations and suggests that the cells were not actively proliferating at the tumor site. This is in agreement with a previous report by Sasportas and colleagues, who found that MSCs persisted at the site of a glioblastoma in vivo, but did not proliferate [22].

Two weeks following MSC-NIS infusion, in vivo imaging confirmed MSC engraftment and functional NIS expression at the target site, with the level of tracer uptake in non-target tissues significantly decreased compared to Day 3. This provided grounds to proceed to ^{131}I therapy. In animals that received an IV injection of MSC-NIS without treatment, mean tumor volume was largest in the study, although not significantly different from MSC free (control) animals. In those that received IT MSC-NIS, tracking of tumor volume revealed no significant effect of ^{131}I therapy. Further analysis of harvested tumor tissue did however reveal increased apoptosis in tumors following direct injection, although to a lesser extent than that observed following IV MSC-NIS delivery. This may be due to the pattern of engraftment of MSCs within the tumor. We and others have previously shown that IT or local injection of MSCs can result in migration and engraftment predominantly around the periphery of the tumor [15, 40]. However, both IT groups displayed decreased tumor volume compared to control animals, suggesting that MSC injection had a negative effect on tumor growth. This is supported by previous studies showing that injection of MSCs into tumor bearing animals resulted in inhibition of tumor growth [40-42].

In the case of IV administration, we had previously reported MSC engraftment throughout breast tumors, apparently lining blood vessels [15]. Beckermann et al. [43] also demonstrated migration of MSCs towards tumor vessels and interaction with the

endothelium. Adipose and bone marrow derived stem cells have also been reported to incorporate into tumor vessels and differentiate into endothelial cells [44] or pericytes [45] respectively. In the current study IV MSC-NIS injection followed by ^{131}I therapy had a cytostatic effect causing a remarkable reduction in the rate of tumor growth, with resulting tumor volumes approximately 75% smaller than their counterpart controls. Histological analysis also revealed significant necrosis in tumor tissues harvested following IV MSC-NIS and therapy. Although not investigated here, this may be as a result of effective targeting of the tumor vasculature. An added safety element to this approach is that ^{131}I therapy will also potentially result in ablation of MSCs, reducing the potential for any negative effects of the cells at the tumor site. Further study is required to investigate persistence of MSCs following therapy, and determine their fate in the tumor microenvironment. There were no adverse effects associated with administration of MSC-NIS (up to 10 weeks) or ^{131}I administration (up to 8 weeks) observed.

These results could conceivably be further improved with a repeat dose of MSC-NIS and radioiodide, as recent studies have shown that tumor irradiation stimulates increased MSC engraftment [7, 46-48]. This may create even greater stimulus for MSC engraftment and treatment of residual disease, which would be particularly attractive in the setting of metastatic disease.

Summary/Conclusion:

This study describes successful exploitation of the dual role of NIS as both a reporter and therapeutic gene following systemic infusion in tumor bearing animals, while using MSCs as tumor-targeted cellular vehicles. The results are extremely promising,

particularly because MSCs target multiple tumor types, and so the approach has potential applications in a range of cancers. The extensive safety record of radioiodide therapy in the treatment of thyroid disease is a major advantage to the use of NIS as a therapeutic gene [16]. In the context of breast cancer, significant inhibition of thyroidal uptake of ^{131}I can be achieved through T_3 supplementation prior to and during ^{131}I therapy [16, 49]. A range of isotopes are efficiently transported by NIS, and are readily available and approved for clinical purposes. Also, gamma camera technology is more widely accessible than more expensive PET scanners. The ability to non-invasively track MSC migration and transgene expression in real time prior to therapy is a major advantage to this strategy. This promising data supports the viability of this approach as a novel therapy for breast cancer.

Acknowledgements: The authors wish to thank Martina Harte for assistance with virus amplification; Georgina Shaw for MSC isolation; Zdzislaw Zuchora for assistance with radionuclides; Emer Hennessy, Catherine Curran and Charles McHale for technical support.

Disclosure of Potential Conflicts of Interest:

The Center for Gamma-Ray Imaging is receiving funding from BioScan, Inc. for development of BazookaSPECT technology.

References

1. Bieback K, Kern S, Kocaomer A, et al. Comparing mesenchymal stromal cells from different human tissues: bone marrow, adipose tissue and umbilical cord blood. Biomed Mater Eng. 2008;18:S71-76.
2. Digirolamo CM, Stokes D, Colter D, et al. Propagation and senescence of human marrow stromal cells in culture: a simple colony-forming assay identifies samples with the greatest potential to propagate and differentiate. Br J Haematol. 1999;107:275-281.
3. Dominici M, Le Blanc K, Mueller I, et al. Minimal criteria for defining multipotent mesenchymal stromal cells. The International Society for Cellular Therapy position statement. Cytotherapy. 2006;8:315-317.
4. Barry FP, Murphy JM. Mesenchymal stem cells: clinical applications and biological characterization. International Journal of Biochemistry & Cell Biology 2004;36:568-584.
5. Wu Y, Wang J, Scott PG, et al. Bone marrow-derived stem cells in wound healing: a review. Wound Repair Regen. 2007;15 Suppl 1:S18-26.
6. Wu Y, Chen L, Scott PG, et al. Mesenchymal stem cells enhance wound healing through differentiation and angiogenesis. Stem Cells. 2007;25:2648-2659.
7. Spaeth E, Klopp A, Dembinski J, et al. Inflammation and tumor microenvironments: defining the migratory itinerary of mesenchymal stem cells. Gene Ther. 2008;15:730-738.
8. Dwyer RM, Khan S, Barry FP, et al. Advances in mesenchymal stem cell-mediated gene therapy for cancer. Stem Cell Res Ther. 2010;1:25.
9. Momin EN, Vela G, Zaidi HA, et al. The Oncogenic Potential of Mesenchymal Stem Cells in the Treatment of Cancer: Directions for Future Research. Curr Immunol Rev. 2010;6:137-148.
10. Ramasamy R, Lam EW, Soeiro I, et al. Mesenchymal stem cells inhibit proliferation and apoptosis of tumor cells: impact on in vivo tumor growth. Leukemia. 2007;21:304-310.
11. Kumar S, Chanda D, Ponnazhagan S. Therapeutic potential of genetically modified mesenchymal stem cells. Gene Ther. 2008;15:711-715.
12. Jemal A, Siegel R, Xu J, et al. Cancer statistics, 2010. CA Cancer J Clin. 2010;60:277-300.
13. Stoff-Khalili MA, Rivera AA, Mathis JM, et al. Mesenchymal stem cells as a vehicle for targeted delivery of CRAds to lung metastases of breast carcinoma. Breast Cancer Research and Treatment. 2007;105 157-167.
14. Studeny M, Marini FC, Dembinski JL, et al. Mesenchymal stem cells: potential precursors for tumor stroma and targeted-delivery vehicles for anticancer agents. Journal of the National Cancer Institute 2004;96:1593-1603.
15. Dwyer RM, Potter-Beirne SM, Harrington KA, et al. Monocyte Chemotactic Protein-1 (MCP-1) secreted by primary breast tumors stimulates migration of Mesenchymal Stem Cells (MSCs). Clin Cancer Res. 2007;13:5020-5027.
16. Mazzaferri E, Kloos R. Current approaches to primary therapy for papillary and follicular thyroid cancer. The Journal of Clinical Endocrinology and Metabolism. 2001;86:1447-1463.

17. Riesco-Eizaguirre G, Santisteban P. A perspective view of sodium iodide symporter research and its clinical implications. Eur J Endocrinol. 2006;155:495-512.
18. Hingorani M, Spitzweg C, Vassaux G, et al. The biology of the sodium iodide symporter and its potential for targeted gene delivery. Curr Cancer Drug Targets. 2010;10:242-267.
19. Dingli D, Diaz RM, Bergert ER, et al. Genetically targeted radiotherapy for multiple myeloma. Gene Therapy. 2003;102:489-496.
20. Kidd S, Spaeth E, Dembinski JL, et al. Direct evidence of mesenchymal stem cell tropism for tumor and wounding microenvironments using in vivo bioluminescent imaging. Stem Cells. 2009;27:2614-2623.
21. Hung SC, Deng WP, Yang WK, et al. Mesenchymal stem cell targeting of microscopic tumors and tumor stroma development monitored by noninvasive in vivo positron emission tomography imaging. Clin Cancer Res. 2005;11:7749-7756.
22. Sasportas LS, Kasmieh R, Wakimoto H, et al. Assessment of therapeutic efficacy and fate of engineered human mesenchymal stem cells for cancer therapy. Proc Natl Acad Sci U S A. 2009;106:4822-4827.
23. Vilalta M, Degano IR, Bago J, et al. Human adipose tissue-derived mesenchymal stromal cells as vehicles for tumor bystander effect: a model based on bioluminescence imaging. Gene Ther. 2009;16:547-557.
24. Wang H, Cao F, De A, et al. Trafficking mesenchymal stem cell engraftment and differentiation in tumor-bearing mice by bioluminescence imaging. Stem Cells. 2009;27:1548-1558.
25. Hwang do W, Jang SJ, Kim YH, et al. Real-time in vivo monitoring of viable stem cells implanted on biocompatible scaffolds. Eur J Nucl Med Mol Imaging. 2008;35:1887-1898.
26. Hwang do W, Kang JH, Jeong JM, et al. Noninvasive in vivo monitoring of neuronal differentiation using reporter driven by a neuronal promoter. Eur J Nucl Med Mol Imaging. 2008;35:135-145.
27. Kim YH, Lee DS, Kang JH, et al. Reversing the silencing of reporter sodium/iodide symporter transgene for stem cell tracking. J Nucl Med. 2005;46:305-311.
28. Terrovitis J, Kwok KF, Lautamaki R, et al. Ectopic expression of the sodium-iodide symporter enables imaging of transplanted cardiac stem cells in vivo by single-photon emission computed tomography or positron emission tomography. J Am Coll Cardiol. 2008;52:1652-1660.
29. Rad AM, Iskander AS, Janic B, et al. AC133+ progenitor cells as gene delivery vehicle and cellular probe in subcutaneous tumor models: a preliminary study. BMC Biotechnol. 2009;9:28.
30. Kakinuma H, Bergert ER, Spitzweg C, et al. Probasin promoter (ARR_2PB)-driven, prostate-specific expression of the human sodium iodide symporter (h-NIS) for targeted radioiodine therapy of prostate cancer. Cancer Research. 2003;15:7840-7844.

31. Livak KJ, Schmittgen TD. Analysis of relative gene expression data using real-time quantitative PCR and the 2(-Delta Delta C(T)) Method. Methods. 2001;25:402-408.
32. Castro RM, Bergert ER, Beito TG, et al. Development of monoclonal antibodies against the human sodium iodide symporter: immunohistochemical characterization of this protein in thyroid cells. The Journal of Clinical Endocrinology and Metabolism. 1999;84:2957-2962.
33. Weiss S, Philip N, Grollman E. Iodine transport in a continuous line of cultured cells from rat thyroid. Endocrinology. 1984;114:1090-1098.
34. Miller BW, Barrett HH, Furenlid LR, et al. Recent advances in BazookaSPECT: Real-time data processing and the development of a gamma-ray microscope. Nucl Instrum Methods Phys Res A. 2008;591:272-275.
35. Dohan O, Baloch Z, Banrevi Z, et al. Predominant intracellular overexpression of the Na^+/I^- symporter (NIS) in a large sampling of thyroid cancer cases. The Journal of Clinical Endocrinology and Metabolism. 2001;86:2697-2700.
36. Dwyer R, Bergert E, O'Connor M, et al. In vivo radioiodide imaging and treatment of breast cancer xenografts following MUC1-driven expression of the sodium iodide symporter (NIS). Clinical Cancer Research. 2005;11:1483-1489.
37. Dwyer RM, Bergert ER, O'Connor MK, et al. Adenovirus-mediated and targeted expression of the sodium-iodide symporter permits in vivo radioiodide imaging and therapy of pancreatic tumors. Hum Gene Ther. 2006;17:661-668.
38. Dwyer RM, Bergert ER, O'Connor MK, et al. Sodium iodide symporter-mediated radioiodide imaging and therapy of ovarian tumor xenografts in mice. Gene Ther. 2006;13:60-66.
39. Nakamizo A, Marini F, Amano T, et al. Human bone marrow-derived mesenchymal stem cells in the treatment of gliomas. Cancer Research. 2005;65:3307-3318.
40. Nakamura K, Ito Y, Kawano Y, et al. Antitumor effect of genetically engineered mesenchymal stem cells in a rat glioma model. Gene Therapy 2004;11:1155-1164.
41. Khakoo AY, Pati S, Anderson SA, et al. Human mesenchymal stem cells exert potent antitumorigenic effects in a model of Kaposi's sarcoma. J Exp Med. 2006;203:1235-1247.
42. Kidd S, Caldwell L, Dietrich M, et al. Mesenchymal stromal cells alone or expressing interferon-beta suppress pancreatic tumors in vivo, an effect countered by anti-inflammatory treatment. Cytotherapy. 2010;12:615-625.
43. Beckermann BM, Kallifatidis G, Groth A, et al. VEGF expression by mesenchymal stem cells contributes to angiogenesis in pancreatic carcinoma. Br J Cancer. 2008;99:622-631.
44. Muehlberg FL, Song YH, Krohn A, et al. Tissue-resident stem cells promote breast cancer growth and metastasis. Carcinogenesis. 2009;30:589-597.
45. Bexell D, Gunnarsson S, Tormin A, et al. Bone marrow multipotent mesenchymal stroma cells act as pericyte-like migratory vehicles in experimental gliomas. Mol Ther. 2009;17:183-190.

46. Klopp AH, Spaeth EL, Dembinski JL, et al. Tumor irradiation increases the recruitment of circulating mesenchymal stem cells into the tumor microenvironment. Cancer Res. 2007;67:11687-11695.
47. Zielske SP, Livant DL, Lawrence TS. Radiation increases invasion of gene-modified mesenchymal stem cells into tumors. Int J Radiat Oncol Biol Phys. 2009;75:843-853.
48. Kim SM, Oh JH, Park SA, et al. Irradiation Enhances the Tumor Tropism and Therapeutic Potential of TRAIL-Secreting Human Umbilical Cord Blood-Derived Mesenchymal Stem Cells in Glioma Therapy. Stem Cells. 2010.
49. Wapnir IL, Goris M, Yudd A, et al. The Na+/I- Symporter mediates iodide uptake in breast cancer metastases and can be selectively down-regulated in the thyroid. Clinical Cancer Research. 2004;10:4294-4302.

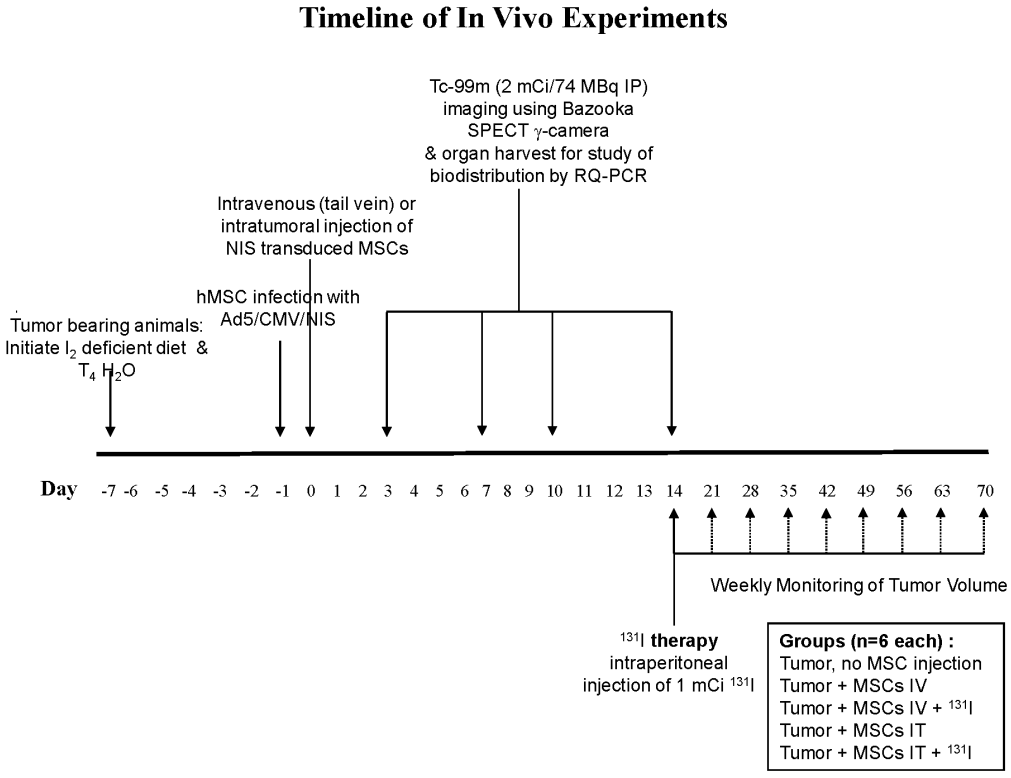

Figure 1: Schematic showing timeline of in vivo MSC-NIS imaging and therapy experiments.

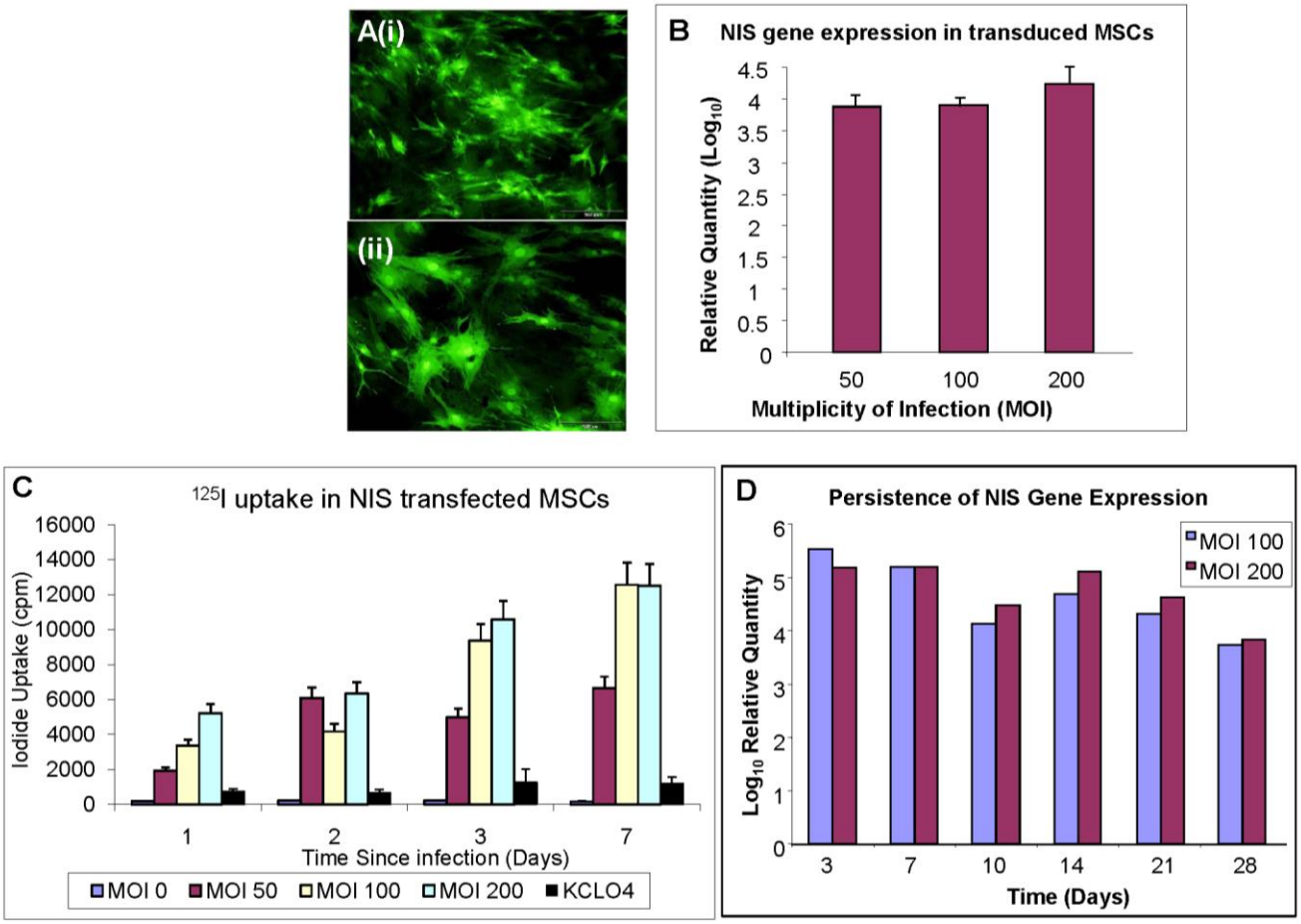

Figure 2: NIS expression and function in AdNIS transduced MSCs **(A)** Adenovirus containing GFP was used to determine transduction efficiency and optimize viral infection conditions, with a fluorescent image of GFP-expressing MSCs from two individual donors shown (i)-(ii). **(B)** Analysis of gene expression in adenovirus infected MSCs. Results are expressed log values relative to uninfected MSCs represented by the baseline **(C)** ^{125}I uptake in MSCs infected with AdNIS at MOI 50-200, 1-7 days following infection. Potassium perchlorate ($KCLO_4$), a specific inhibitor of NIS function, was included in control wells. **(D)** Persistence of NIS gene expression in MSCs up to 28 days following AdNIS infection.

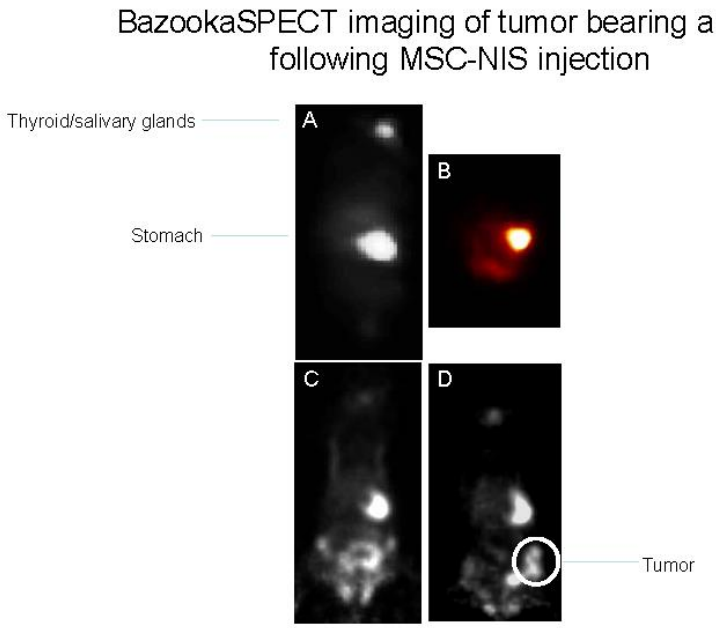

Figure 3: In vivo MDA-MB-231 tumor imaging of mice using a BazookaSPECT γ-camera after administration of 2 mCi/74 MBq technetium-99m pertechnetate ($^{99m}TcO_4^-$). (**A**) Single coronal slice of volume rendering from a reconstructed SPECT image of a control animal-(MSC free). This revealed an image showing $^{99m}TcO_4^-$ uptake in the thyroid and stomach, which both express endogenous NIS. **(B)** Single transverse slice of volume rendering from a reconstructed SPECT image of a tumor 3 days following intratumoral injection of MSC-NIS, showing robust uptake of tracer. (**C, D**) Planar images of tumor bearing animals 3 days **(C)** or 14 days **(D)** following intravenous injection of MSC-NIS. **(C)** revealed a pattern of uptake apparently correlating with the location of the intestines, and also diffuse uptake in the chest area. A weak image of the right flank tumor can also be observed. **(D)** Imaging 14 days following MSC-NIS injection revealed a clear image of the right flank tumor, with a significant reduction in ectopic concentration of tracer in non-target tissue observed. In some cases the bladder is also visible, where $^{99m}TcO_4^-$ was being excreted in urine.

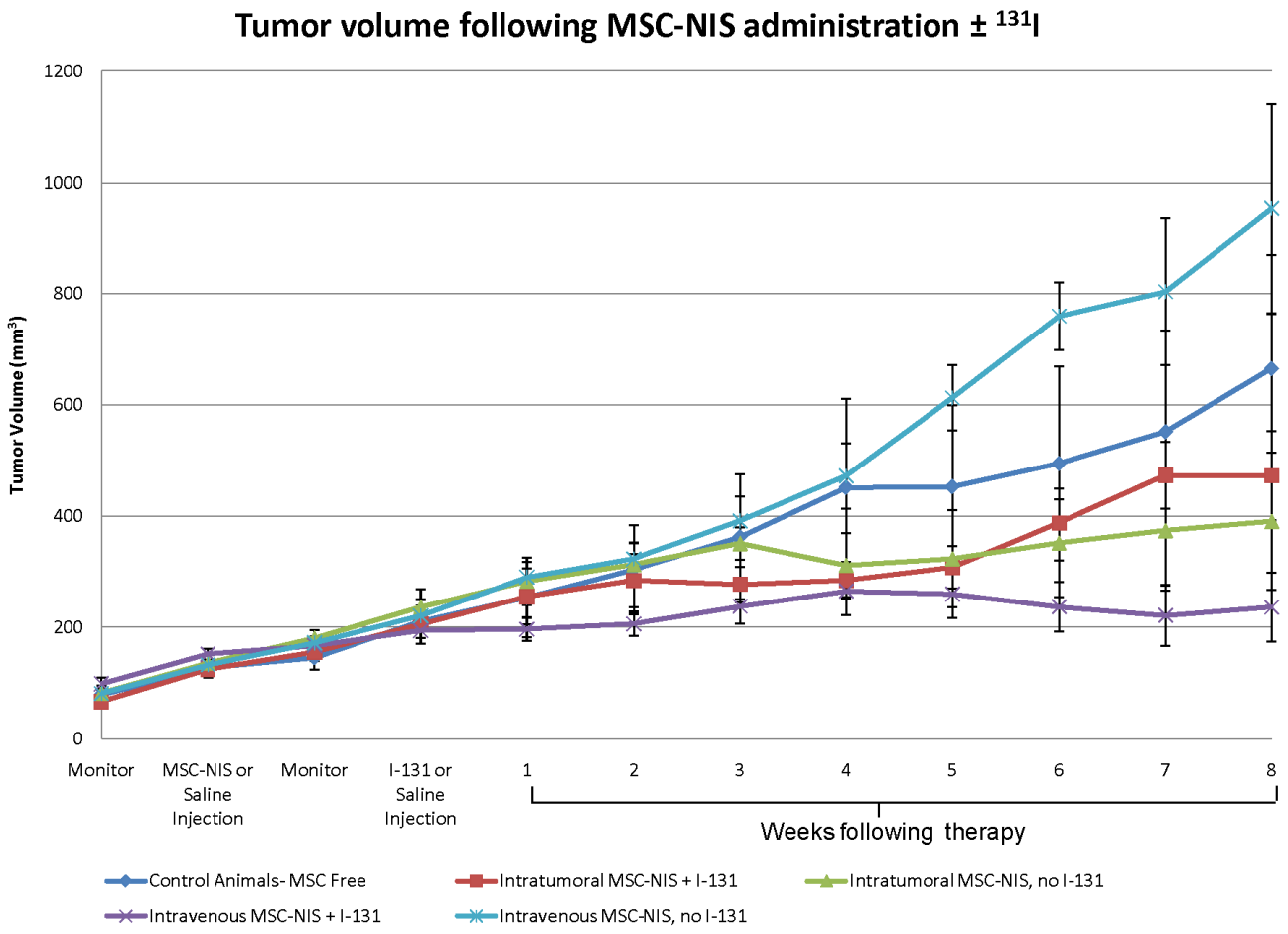

Figure 4: In vivo radioiodine therapy of MDA-MB-231 breast tumor xenografts 14 days following injection of MSC-NIS. Animals received an intratumoral or intravenous injection of NIS-expressing MSCs followed by an intraperitoneal dose of either ^{131}I or saline 14 days late.

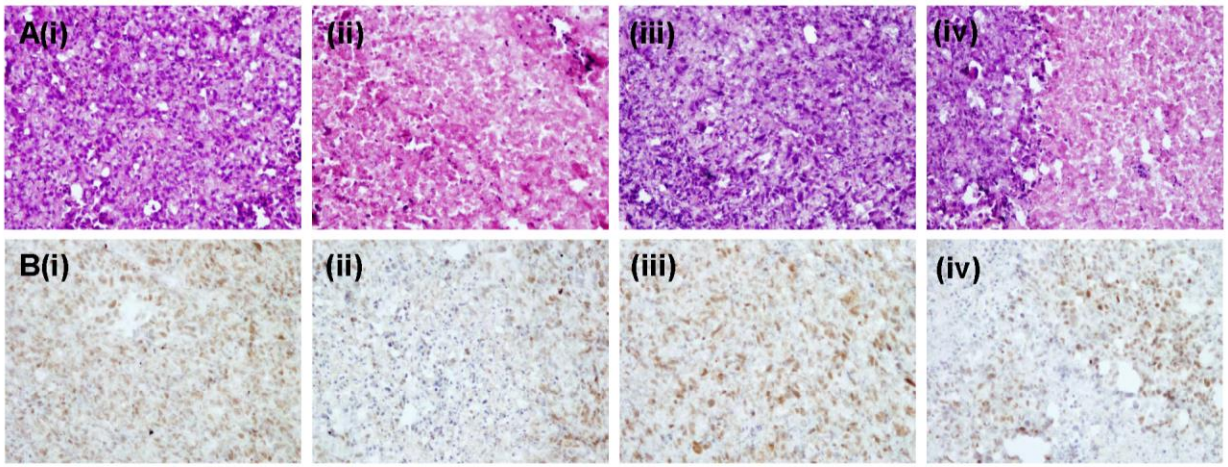

Figure 5: Histology and immunohistochemistry of tumor tissue harvested from mice 8 weeks following administration of ^{131}I or saline (10 weeks following MSC-NIS injection). Row A: H & E staining (200X), Row B: PCNA detection by immunohistochemistry (200X). Columns- (i) Intravenous (IV) MSC-NIS + saline (ii) IV MSC-NIS + ^{131}I (iii) Intratumoral (IT) MSC-NIS + saline (iv) IT MSC-NIS + ^{131}I

Tissue	**Intravenous AdNIS**				**Intravenous MSC-NIS**			
	hNIS		hMRPL19		hNIS		hMRPL19	
	Day3	Day7	Day3	Day7	Day3	Day7	Day3	Day7
Tumor	-	-	+	+	++	++	++	++
Heart	+	-	-	-	++	+	++	+
Lungs	+	-	-	-	++	+	++	+
Liver	+	-	-	-	+	-	-	-
Spleen	-	-	-	-	-	-	-	-
Kidneys	-	-	-	-	-	-	-	-
Stomach	-	-	-	-	-	-	-	-
Small Intestine	-	-	-	-	-	-	-	-
Large Intestine	-	-	-	-	+	+	+	+

Table 1: Detection of human *NIS* and *MRPL19* expression in animal tissues 3 and 7 days following intravenous administration of either naked virus (AdNIS) or adenovirus infected MSCs (MSC-NIS). (-) Not detectable (+) low levels of gene expression detected (++) more robust gene expression detected.